Multi-Task Semi-Supervised Learning for Vascular Network Segmentation and Renal Cell Carcinoma Classification

Rudan Xiao, Damien Ambrosetti, Xavier Descombes

Multi-Task Semi-Supervised Learning for Vascular Network Segmentation and Renal Cell Carcinoma Classification

Rudan Xiao[1], Damien Ambrosetti[2], and Xavier Descombes[1]

[1] Université Côte d'Azur, Inria, CNRS, I3S, France
[2] Hôpital Pasteur, CHU Nice, France

Abstract. Vascular network analysis is crucial to define the tumoral architecture and then diagnose the cancer subtype. However, automatic vascular network segmentation from Hematoxylin and Eosin (H&E) staining histopathological images is still a challenge due to the background complexity. Moreover, there is a lack of large manually annotated vascular network databases. In this paper, we propose a method that reduces reliance on labeled data through semi-supervised learning (SSL). Additionally, considering the correlation between tumor classification and vascular segmentation, we propose a multi-task learning (MTL) model that can simultaneously segment the vascular network using SSL and predict the tumor class in a supervised context. This multi-task learning procedure offers an end-to-end machine learning solution to joint vascular network segmentation and tumor classification. Experiments were carried out on a database of histopathological images of renal cell carcinoma (RCC) and then tested on both own RCC and open-source TCGA datasets. The results show that the proposed MTL-SSL model outperforms the conventional supervised-learning segmentation approach.

Keywords: Vascular Network Segmentation · Semi-Supervised Learning · Multi-Task Learning · Renal Cell Carcinoma

1 Introduction

85% to 90% of kidney cancer are RCC, with the main subtypes being clear cell RCC (ccRCC) with 75%, papillary RCC (pRCC) with 10% and Chromophobe with 5% [11]. Currently, subtyping is essentially based upon pathological analysis, consisting of cell morphology and tumor architecture [8]. [24] proved vascular network analysis is important and relevant in RCC subtyping, however this classification work only used a few manually segmented vascular networks, which limits its application potential. In this paper, we propose to build an automatic vascular network segmentation model paired with a tumor classification scheme.

Data labeling is often the most challenging task. Labeling large-scale images are laborious, time-consuming and exhibit low repeatability. This encouraged to improve the vascular network segmentation performance using unlabeled data.

This is indeed the paradigm of SSL models. Compared with the difficulty of obtaining manually a vascular network mask for the segmentation task, the labeling for the classification task is easy to obtain. We conjectured that joint supervised classification and SSL for vascular network segmentation, both embedded in a MTL model, may improve the performance of vascular network segmentation in RCC histopathological images.

We conducted benchmark experiments of supervised learning, SSL, both single and multi-tasks, on RCC histopathological images. Then test on RCC and other types of tumors. The proposed MTL-SSL model performs best, outperforming and more robust than the fully supervised learning model. Moreover, compared with the single-task SSL, our model indeed improves the segmentation efficiency of the vascular network while also performing tumor classification.

Our contributions can be summarized as follows:

- We propose an MTL-SSL model performing joint SSL segmentation and classification tasks to segment the vascular network using both labeled and unlabeled data.
- We apply the first automatic, end-to-end vascular network segmentation method in H&E staining histopathological images, which is robust and outperforms the fully supervised model on both RCC new subtype and other cancer datasets.
- The proposed MTL-SSL model forms a foundation for future developments in multi-task learning dealing with vascular segmentation and classification from H&E staining histopathological images.

2 Related works

SSL [6] plays a key role in segmentation tasks since it allows to reduce the reliance on large annotated datasets. It can provide an effective way of leveraging unlabeled data to improve model performance. Several approaches have been proposed for SSL, such as Deep Adversarial Networks [26], Cross Pseudo Supervision [7], Cross Consistency Training [15] and Mean Teacher [21]. However, only a few studies have investigated if SSL can be applied to achieve satisfactory results in H&E staining histopathological images, such as NAS-SGAN [9] for atypia scoring of breast cancer, OSE-SSL [18] for content-based image retrieval of prostate cancer, and breast cancer classification with Self-Paced Learning together [2]. In this paper, we apply SSL to RCC histopathological images to provide the benchmarks for vascular network segmentation.

MTL [4] aims at improving the performance of multiple related learning tasks by leveraging comprehensive information among them. MTL achieves better generalization properties than single-task learning. Classification and segmentation are both key tasks in medical image processing. Joint segmentation and classification of tumors in 3D automated breast ultrasound images shows that learning these two tasks simultaneously improves the outcomes of both tasks [27]. Other joint tasks using MTL in cell detection and segmentation on PMS2 stained colon rectal cancer and tonsil tissue images [5], MitosisNet for mitosis detection from

pathological images which consist of segmentation, detection and classification models [1], etc. In this paper, we combine the classification task for which labels are easy to obtain and the vascular network segmentation task for which images have complex backgrounds and manual delineation is cumbersome. Our MTL aims to improve the performance of the segmentation task on RCC histopathological images compared to the fully supervised learning task.

Vasculature from histological images plays a key role in cancer development subtyping and radiotherapy assessment [13]. However, the current automatic vascular segmentation for histopathological images is limited to Immunohistochemistry (IHC) stained histology images. [3] segments and quantify blood vessels from hematoxylin and diaminobenzidine (H&DAB) stained histopathological images of Alzheimer's disease. [12] obtained vascular hotspot probability maps of WSI by scanning whole CD34 immunostained histological images of colon cancer samples. Using H& DAB staining for special coloration of blood vessels, the background is clean and easy to segment, but the background of the H&E image is more complex and has some similar linear structures, such as cell membranes and fibers, etc., which makes the task of vascular segmentation from H&E images more challenging. In this paper, we propose an MTL-SSL model which can segment vascular networks from H&E staining histopathological images automatically while predicting the tumor class.

3 Dataset and Methods

3.1 Dataset Building

We followed the method of [24] to annotate vascular. This weak label is faster and embeds the topological information of the vascular, which has been shown sufficient for the classify subtypes of RCC. Although the width of vascular vessels is lost as we consider to represent the vascular by that way, shown in Figure 1.

For our own RCC dataset, We collected 167 original H&E staining WSI and labeled the tumor and non-tumor areas using the software ASAP to obtain patches of 2000×2000 Pixels. The pipeline is shown in Figure 1. We obtain 42130 tumor patches (27287 of ccRCC, 13637 of pRCC, 1206 of Chromophobe), and manually labeled 424 vascular masks (129 of ccRCC, 129 of pRCC, 166 of Chromophobe) for train and test and then labeled 12 masks of Oncocytoma, which is another subtype of RCC, only for test the robustness of the segmentation.

For the TCGA dataset, we downloaded 100 WSIs of RCC (only have ccRCC and pRCC), breast cancer, lung cancer, liver cancer, and esophagus cancer. Then got 1029 tumor patches (433 of RCC, 60 of breast cancer, 246 of liver cancer, 120 of lung cancer, and 170 of esophagus cancer). We manually labeled 90 vascular network masks (20 of RCC, 15 of breast cancer, 20 of liver cancer, 20 of lung cancer, and 15 of esophagus cancer) only for test.

3.2 Multi-Task Learning Pipeline

Our proposed MTL-SSL model has a shared backbone encoder with task-specific heads. It consists of a classification task in supervised learning context and a seg-

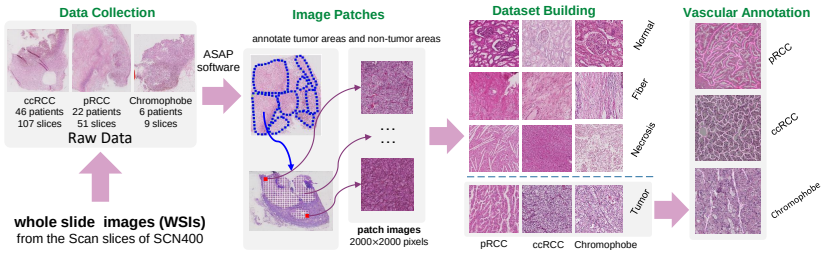

Fig. 1. RCC histopathological images dataset.

mentation task using SSL, as shown in Figure 2. We chose HRNet [19] as the backbone after comparison with other models. HRNet backbone [19] can output high-resolution feature maps. It starts with a high-resolution subnetwork as the first stage, and gradually adds high-to-low resolution subnetworks, forming more stages, and connecting the multi-resolution subnetworks in parallel. HRNet segmentation heads (student and teacher heads) aggregate the output representations at four different resolutions, and then use a 1x1 convolutions to fuse these representations. HRNet classification head fed the four-resolution feature maps into a bottleneck and the number of output channels are increased to 128, 256, 512, and 1024, respectively, and transform 1024 channels to 2048 channels through a 1x1 convolution finally. The codes of Multi-task and HRNet backbone were developed according to the shared repositories [22] and [19]. The main hyperparameters used in our paper are the same as in [22] and [19]. Ensuring fair comparison, all the models were trained using the same hyperparameters.

We chose the Mean Teacher [21] for SSL, which has two neural networks of student and teacher modules sharing the same architecture. Both the student and the teacher module evaluate the input slightly perturbed with Gaussian noise (ξ and ξ') within their computation. The weights of the student module are updated using the Adam optimizer, whereas the weights of the teacher module are the Exponential Moving Average (EMA) of the student weights. We use the cross-entropy (CE) and Dice loss functions between the student's predictions and the ground-truth on the labeled dataset to get *loss2*. The consistency cost, called *loss3* here, is computed from the student's prediction and the teacher's prediction by Mean Square Error (MSE) on the unlabeled dataset. The semi-supervised *loss4* is the sum of the supervised *loss2* and the consistency cost *loss3* by consistency weights, which were taken from [21]. Classification *loss1* is computed by the CE function on the class labeled dataset. Final *loss5* of our MTL-SSL model is the weighted sum of semi-supervised *loss4* and classification *loss1*, we define the weight ratio of SSL and classification as 2:1.

3.3 Evaluation

The weakly label of the vascular network has been made with constant width bands[24]. Shown as Figure 3, the generated vascular segmentation is even closer

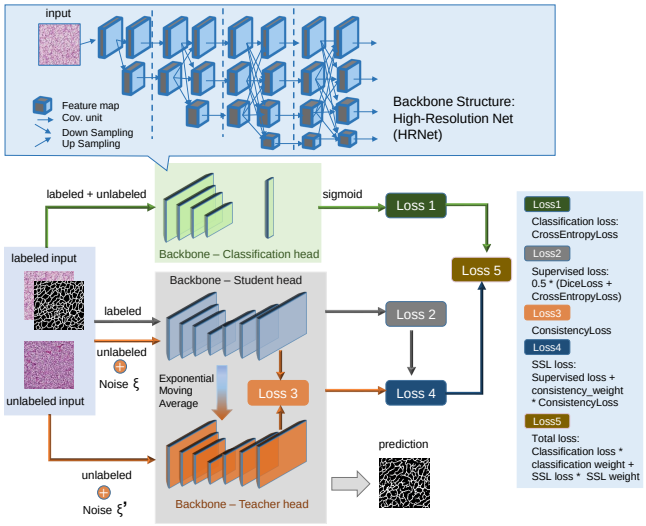

Fig. 2. Proposed MTL-SSL model architecture.

to the real vascular mask than the weakly labeled ground truth. The classical evaluation indexes such as Dice or Jaccard are not relevant here due to false positive and negative pixels appear at the border of a vessel. To overcome this imprecise ground truth we proposed the following post-processing to evaluate the results in terms of vessel detection, basically to consider length but not the width of vessels. We dilated (with a disk of radius 3, according to Table 1) the segmentation result S to obtain DS and the ground truth GT to obtain DGT. We computed the ratio of miss-detected vessels as:

$$MV = \frac{|\{(i,j) : GT(i,j) = 1, DS(i,j) = 0\}|}{|\{(i,j) : GT(i,j) = 1\}|} \tag{1}$$

and the ratio of falsely detected vessels as:

$$FV = \frac{|\{(i,j) : S(i,j) = 1, DGT(i,j) = 0\}|}{|\{(i,j) : S(i,j) = 1\}|}. \tag{2}$$

Finally, we defined the following global performance index:

$$IV = 1 - (MV + VF)/2 \tag{3}$$

4 Experiments and Results

In this section, we launch the benchmark experiments for vascular network segmentation with different models and also do the statistical analysis of the differences in the results between our proposed model and other models using the

Table 1. Evaluate with different Strel Radius.

Radius	MV(↓)	FV(↓)	IV(↑)
1	0.1353(0.02)	0.3514(0.06)	0.7566(0.02)*
2	0.1208(0.02)	0.3361(0.06)	0.7716(0.02)*
3 (Our)	0.2798(0.02)	**0.1243(0.03)**	**0.7979(0.01)**
4	0.1040(0.02)	0.3205(0.06)	0.7878(0.02)
5	**0.0835(0.02)**	0.3426(0.04)	0.7870(0.01)

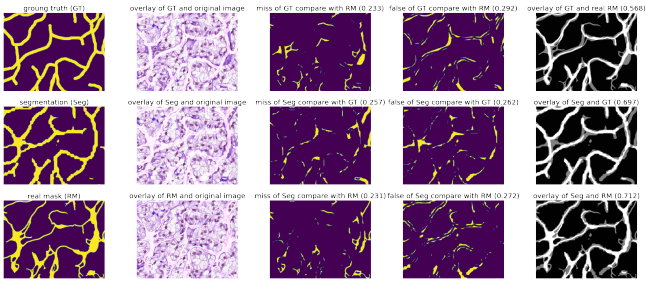

Fig. 3. Calculate the missing part and the false part between the generated segmentations, weakly labels, and real vascular masks by comparing them.

student's t-test. The statistical software SPSS, version 20.0, was used for all the statistical analyses. The level for statistical significance was set $\alpha = 0.05$. *: significantly worse than HRNet backbone or our proposed model (P <0.05).

4.1 Backbone and MTL-SSL method choice

We conducted experiments on different supervised classification models (GoogLeNet [20], ShuffleNet [25], VggNet [17], ResNet [10] and HRNet [19]) and competitive SSL models (Cross Pseudo Supervision (CPS) [7], Cross Consistency Training (CCT) [15], Entropy Minimization (EM) [23] Deep Co-Training (DCT) [16] and Mean Teacher (MT) [21]) to select the more efficient backbone. For the classification, we split our database into train input with 18624 tumor patch images (8913 of ccRCC, 9079 of pRCC and 632 of Chromophobe), validation with 4843 tumor patch images (2049 of ccRCC, 2523 of pRCC and 271 of Chromophobe), and test with 6973 tumor patch images (4420 of ccRCC, 2250 of pRCC and 303 of Chromophobe). For train input of SSL segmentation, we used both the labeled vascular masks of our dataset with 335 tumor patch images (112 of ccRCC, 111 of pRCC and 112 of Chromophobe) and the 1005 unlabeled data from the RCC dataset randomly, which is 3 times the labeled data. Meanwhile the validation of SSL with 32 tumor patch images (8 of ccRCC, 9 of pRCC and 15 of Chromophobe) and test with 69 tumor patch images (9 of ccRCC, 9 of pRCC, 39 of Chromophobe and 12 of Oncocytoma) selected randomly. All the experiments have been repeated 5 times. The mean and standard deviation of the different model results are shown in Table 2. HRNet backbone performed best in both

classification and SSL segmentation tasks. And MTL-SSL based on mean teacher reaches the best performance among all the segmentation methods. All the code and parameters are from the open repository SSL4MIS [14].

Table 2. Performence of different backbones.

Methods			Backbone	Accuracy	
Classification			GoogLeNet	0.9348(0.01)	
			ShuffleNet	0.7753(0.07)*	
			VggNet	0.9114(0.01)	
			ResNet	0.8863(0.03)	
			DenseNet	0.762(0.001)*	
			HRNet	**0.9369(0.03)**	
Method			Backbone	MV(↓)	FV(↓)	IV(↑)
SSL Segmentation	DCT (ECCV 2018)	Single Task	UNet	0.3770(0.02)	0.7453(0.05)	0.4388(0.02)*
	EM (CVPR 2019)		UNet	0.3340(0.04)	0.7686(0.01)	0.4487(0.02)*
	CCT (CVPR2020)		UNet	0.3644(0.03)	0.7474(0.03)	0.4417(0.004)*
	CPS (CVPR 2021)		UNet	0.3459(0.01)	0.7467(0.01)	0.4537(0.01)
	MT (NIPS 2017)		UNet	0.3622(0.002)	0.7827(0.002)	0.4275(0.001)*
	DCT (ECCV 2018)		HRNet	0.2926(0.02)	0.7846(0.01)	0.4614(0.004)
	EM (CVPR 2019)		HRNet	0.3049(0.01)	0.7844(0.01)	0.4554(0.01)
	CCT (CVPR2020)		HRNet	0.2842(0.02)	0.7951(0.01)	0.4604(0.01)
	CPS (CVPR 2021)		HRNet	0.3190(0.02)	0.7733(0.01)	0.4539(0.01)
	MT (NIPS 2017)		HRNet	0.2934(0.02)	0.7932(0.01)	0.4567(0.01)
	DCT (ECCV 2018)		HRNet	0.3032(0.01)	0.1073(0.02)	0.7948(0.01)
	EM (CVPR 2019)		HRNet	0.1307(0.04)	0.2893(0.06)	0.7900(0.01)
	CCT (CVPR2020)	Multi Task	HRNet	0.1562(0.05)	0.4189(0.05)	0.7209(0.05)*
	CPS (CVPR 2021)		HRNet	0.2142(0.03)	0.8455(0.01)	0.4702(0.02)*
	MT (NIPS 2017) **Our**		HRNet	0.2798(0.02)	0.1243(0.03)	**0.7979(0.01)**

4.2 Segmentation Benchmarks of Vascular Network

We conducted benchmark experiments on supervised learning, SSL, single segmentation task and MTL. For SSL, the data split ratios were the same as in the backbone choice experiment. For supervised learning, we only used the 335 labeled data for train input, 32 for validation and 69 for test. All the data were selected randomly. For the common parameter setup, the input size was 512×512 pixels, the optimizer was Adam. We used batches of size 8, epoch of 200 and a poly learning rate decay scheme. The initial learning rate was 0.002 and weight decay was 1×10^{-6}. For the parameter setup specific to SSL, the ema decay was 0.99, the consistency type was "mse", the consistency was 0.1, and the consistency rampup was 50. In addition, we also compare the segmentation results of our MTL-SSL and fully supervised models under different scales of labeled data.

Figure 4 shows the segmentation results of MTL-SSL and Table 3 gives a quantitative evaluation. The proposed MTL-SSL model reaches the best perfor-

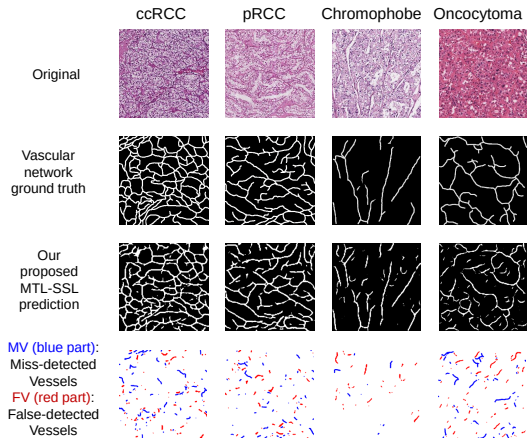

Fig. 4. Segmentation results of the proposed MTL-SSL model.

Table 3. Performance of different models.

Supervised	**MV(↓)**	**FV(↓)**	**IV(↑)**
single-task	**0.2551(0.02)**	0.1600(0.03)	0.7924(0.01)
multi-task	0.3119(0.05)	**0.1032(0.01)**	0.7925(0.02)
Semi-Supervised	**MV(↓)**	**FV(↓)**	**IV(↑)**
single-task	0.2934(0.02)	0.7932(0.01)	0.4567(0.01)*
multi-task (Our)	0.2798(0.02)	0.1243(0.03)	**0.7979(0.01)**

mance among all the experiments. And Table 4 shows the smaller the scale of the labeled data, the more advantages of our MTL-SSL model.

4.3 Test on new subtype of RCC and other cancers dataset.

Figure 5 shows the segmentation results of MTL-SSL on TCGA dataset. And Table 5 shows MTL-SSL model is more robust than fully supervised segmentation when considering new subtype and other cancers test. Our MTL-SSL model appears to be versatile with respect to vascular segmentation tasks, it has the potential to segment vascular from other subtypes of RCC and even other

Table 4. Performance of different labeled data in training.

		Labeled=200	**Labeled=300**	**Labeled=all (335)**
Supervised Task	MV(↓)	**0.091(0.01)**	0.1067(0.02)	**0.2551(0.02)**
	FV(↓)	0.4120(0.02)	0.3670(0.03)	0.1600(0.03)
	IV(↑)	0.7483(0.01)*	0.7631(0.01)	0.7924(0.01)
Semi-Supervised Multi-task (Our)	MV(↓)	0.1100(0.02)	**0.1046(0.004)**	0.2798(0.02)
	FV(↓)	**0.3580(0.04)**	**0.3302(0.03)**	**0.1243(0.03)**
	IV(↑)	**0.7660(0.01)**	**0.7826(0.02)**	**0.7979(0.01)**

Table 5. Performance of new subtype of RCC and other cancers.

Task	Dataset	MV(↓)	FV(↓)	IV(↑)
Supervised Task	Our-RCC (new subtype)	**0.1366(0.03)**	0.4501(0.04)	0.7067(0.01)*
	TCGA-RCC (2 subtypes)	0.087(0.01)	0.1746(0.03)	0.8691(0.01)
	TCGA-BRCA (breast)	0.2179(0.05)	0.3892(0.21)	0.6965(0.10)*
	TCGA-LIHC (liver)	0.1720(0.02)	0.3177(0.03)	0.7551(0.02)*
	TCGA-LUSC (lung)	**0.1865(0.02)**	0.2847(0.04)	0.7644(0.02)*
	TCGA-ESCA (esophagus)	0.1734(0.02)	0.2792(0.03)	0.7737(0.01)*
Semi-Supervised Multi-Task (Our)	Our-RCC (new subtype)	0.1631(0.02)	**0.2635(0.04)**	**0.7867(0.01)**
	TCGA-RCC (2 subtypes)	**0.068(0.01)**	**0.1746(0.02)**	**0.8786(0.01)**
	TCGA-BRCA (breast)	**0.1863(0.03)**	**0.3301(0.1)**	**0.7418(0.03)**
	TCGA-LIHC (liver)	**0.1483(0.03)**	**0.2262(0.08)**	**0.8127(0.03)**
	TCGA-LUSC (lung)	0.1930(0.02)	**0.1910(0.07)**	**0.8080(0.03)**
	TCGA-ESCA (esophagus)	**0.1663(0.02)**	**0.2419(0.08)**	**0.7959(0.03)**

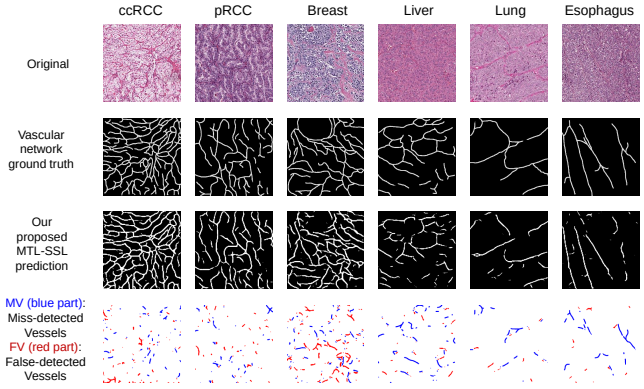

Fig. 5. Segmentation results of the proposed MTL-SSL model on TCGA dataset.

cancers without adding manual vascular masks for training. This provides foundation for the study of the vascular networks in H&E staining histopathological images, which is not limited to immunostaining and manual labeling.

Furthermore, segmentation of vascular networks in H&E histopathology images is very challenging, in this context, our MTL-SSL model has improved state of the art by HRNet backbone, loss strategy, and MTL with classification.

5 Conclusion

The proposed MTL-SSL model, trained with both labeled and unlabeled data, reduces the reliance on manually vascular network masks and achieves automatic segmentation. In our experiments, this model can outperform the fully supervised learning model and is versatile in other types of tumors. That clarified applying the HRNet backbone-based multitask model (jointly with an SSL principle) to vascular segmentation of histopathological images is valuable.

References

1. Alom, M.Z., Aspiras, T., Taha, T.M., Bowen, T., Asari, V.K.: Mitosisnet: end-to-end mitotic cell detection by multi-task learning. IEEE Access **8**, 68695–68710 (2020)
2. Asare, S.K., You, F., Nartey, O.T.: A semisupervised learning scheme with self-paced learning for classifying breast cancer histopathological images. Computational Intelligence and Neuroscience **2020** (2020)
3. Bukenya, F., Nerissa, C., Serres, S., Pardon, M.C., Bai, L.: An automated method for segmentation and quantification of blood vessels in histology images. Microvascular Research **128**, 103928 (2020)
4. Caruana, R.: Multitask learning. Machine learning **28**(1), 41–75 (1997)
5. Chamanzar, A., Nie, Y.: Weakly supervised multi-task learning for cell detection and segmentation. In: ISBI. pp. 513–516. IEEE (2020)
6. Chapelle, O., Scholkopf, B., Zien, A.: Semi-supervised learning. IEEE Transactions on Neural Networks **20**(3), 542–542 (2009)
7. Chen, X., Yuan, Y., Zeng, G., Wang, J.: Semi-supervised semantic segmentation with cross pseudo supervision. In: CVPR. pp. 2613–2622 (2021)
8. Cheville, J.C., Lohse, C.M., Zincke, H., Weaver, A.L., Blute, M.L.: Comparisons of outcome and prognostic features among histologic subtypes of renal cell carcinoma. The American journal of surgical pathology **27**(5), 612–624 (2003)
9. Das, A., Devarampati, V.K., Nair, M.S.: Nas-sgan: A semi-supervised generative adversarial network model for atypia scoring of breast cancer histopathological images. IEEE Journal of Biomedical and Health Informatics (2021)
10. He, K., Zhang, X., Ren, S., Sun, J.: Deep residual learning for image recognition. In: CVPR. pp. 770–778 (2016)
11. Hsieh, J.J., Purdue, M.P., Signoretti, S., Swanton, C., Albiges, L., Schmidinger, M., Heng, D.Y., Larkin, J., Ficarra, V.: Renal cell carcinoma. Nature reviews Disease primers **3**(1), 1–19 (2017)
12. Kather, J.N., Marx, A., Reyes-Aldasoro, C.C., Schad, L.R., Zöllner, F.G., Weis, C.A.: Continuous representation of tumor microvessel density and detection of angiogenic hotspots in histological whole-slide images. Oncotarget **6**(22), 19163 (2015)
13. Loukas, C.G., Linney, A.: A survey on histological image analysis-based assessment of three major biological factors influencing radiotherapy: proliferation, hypoxia and vasculature. Computer Methods and Programs in Biomedicine **74**(3), 183–199 (2004)
14. Luo, X.: SSL4MIS. https://github.com/HiLab-git/SSL4MIS (2020)
15. Ouali, Y., Hudelot, C., Tami, M.: Semi-supervised semantic segmentation with cross-consistency training. In: CVPR. pp. 12674–12684 (2020)
16. Qiao, S., Shen, W., Zhang, Z., Wang, B., Yuille, A.: Deep co-training for semi-supervised image recognition. In: ECCV. pp. 135–152 (2018)
17. Simonyan, K., Zisserman, Andrew: Very deep convolutional networks for large-scale image recognition. arXiv (2014)
18. Sparks, R., Madabhushi, A.: Out-of-sample extrapolation utilizing semi-supervised manifold learning (ose-ssl): Content based image retrieval for histopathology images. Scientific reports **6**(1), 1–15 (2016)
19. Sun, K., Xiao, B., Liu, D., Wang, J.: Deep high-resolution representation learning for human pose estimation. In: CVPR. pp. 5693–5703 (2019)

20. Szegedy, C., Liu, W., Jia, Y., Sermanet, P., Reed, S., Anguelov, D., Erhan, D., Vanhoucke, V., Rabinovich, A.: Going deeper with convolutions. In: CVPR. pp. 1–9 (2015)
21. Tarvainen, A., Valpola, H.: Mean teachers are better role models: Weight-averaged consistency targets improve semi-supervised deep learning results. arXiv (2017)
22. Vandenhende, S., Georgoulis, S., Gool, L.V.: Mti-net: Multi-scale task interaction networks for multi-task learning. In: ECCV. pp. 527–543. Springer (2020)
23. Vu, T.H., Jain, H., Bucher, M., Cord, M., Pérez, P.: Advent: Adversarial entropy minimization for domain adaptation in semantic segmentation. In: CVPR. pp. 2517–2526 (2019)
24. Xiao, R., Debreuve, E., Ambrosetti, D., Descombes, X.: Renal cell carcinoma classification from vascular morphology. In: MICCAI. pp. 611–621. Springer (2021)
25. Zhang, X., Zhou, X., Lin, M., Sun, J.: Shufflenet: An extremely efficient convolutional neural network for mobile devices. In: CVPR. pp. 6848–6856 (2018)
26. Zhang, Y., Yang, L., Chen, J., Fredericksen, M., Hughes, D.P., Chen, D.Z.: Deep adversarial networks for biomedical image segmentation utilizing unannotated images. In: MICCAI. pp. 408–416. Springer (2017)
27. Zhou, Y., Chen, H., Li, Y., Liu, Q., Xu, X., Wang, S., Yap, P.T., Shen, D.: Multi-task learning for segmentation and classification of tumors in 3d automated breast ultrasound images. Medical Image Analysis **70**, 101918 (2021)